Biomedical Signal Processing and Control 24 (2016) 120–127

Contents lists available at ScienceDirect

Biomedical Signal Processing and Control

journal homepage: www.elsevier.com/locate/bspc

Denoising optical coherence tomography using second order total generalized variation decomposition

Jinming Duan [a,*], Wenqi Lu [b], Christopher Tench [c], Irene Gottlob [d], Frank Proudlock [d], Niraj Nilesh Samani [d], Li Bai [a]

[a] School of Computer Science, University of Nottingham, UK
[b] College of Information Engineering, Qingdao University, China
[c] School of Medicine, University of Nottingham, UK
[d] Ophthalmology Department, University of Leicester, UK

ARTICLE INFO

Article history:
Received 11 May 2015
Received in revised form 8 September 2015
Accepted 30 September 2015
Available online 6 November 2015

Keywords:
Optical coherence tomography
Variational methods
Image decomposition
Noise removal
Total generalised variation
Split Bregman algorithm
Fast Fourier transform

ABSTRACT

In this paper, we apply image decomposition for image denoising by considering the speckle noise in the (OCT) image as texture or oscillatory patterns. A novel second order total generalised variation (TGV) decomposition model is proposed to remove noise (texture) from the OCT image. The incorporation of the TGV regularisation in the proposed model can eliminate the staircase side effect in the resulting denoised image (structure). By introducing auxiliary splitting variables and Bregman iterative parameters, a fast Fourier transform based split Bregman algorithm is developed to solve the proposed model explicitly and efficiently. Extensive experiments are conducted on both synthetic and real OCT images to demonstrate that the proposed model outperforms state-of-the-art speckle noise reduction methods.

1. Introduction

Optical coherence tomography (OCT) is a non-invasive imaging modality and plays an important role in clinical diagnosis and monitoring of diseases of the retina. However, as with other imaging modalities based on the detection of coherence sources, OCT images are always corrupted by speckle noise, which can mask image features and pose significant challenges for image analysis algorithms [1]. Intensity fluctuation and motion artifact also decrease image quality, and presence of blood vessels in the image makes layer boundaries appear discontinuous. Thus pre-processing is often the first step in OCT image analysis.

There are mainly two classes of methods for speckle noise reduction of OCT images. The first class of methods use physical techniques, such as the frequency compounding and polarization diversity [2–4], to address the noise problem before final image formation. However, these methods require significant modifications to design of the OCT system and can be too complicated and expensive to apply in practise. The second class of methods rely on post-processing of images and representatives of this class include filter based and diffusion based approaches.

Adaptive adaptive filters calculate the value of each pixel using the information in the local neighbourhood of the pixel. These include hybrid median filter [5], homomorphic Wiener filter [6], enhanced Lee filter [7], symmetric nearest neighbour filter [8], Kuwahara filter [9], etc. Wavelet-based filters have the advantage of denoising on multiscale resolutions and are more desirable for dealing with correlated noise. Ozcan et al. [10] compared standard digital denoising methods and concluded that wavelet thresholding with the shift invariant wavelets yielded the best results. A spatially adaptive wavelet filter was described in [11], where a set of statistical wavelet coefficients were applied to estimate the thresholds for denoising OCT images. Mayer et al. [12] proposed a wavelet denoising algorithm for OCT images. The wavelet coefficients are first calculated based on local noise and structure estimation, and then weighted, averaged and used to reconstruct the denoised image. Puvanathasan et al. [13] proposed a type-II fuzzy thresholding algorithm for choosing wavelet filtering thresholds. Modern wavelets such as the dual tree complex wavelet [14] and curvelet transform [15] have also been employed to remove speckle noise from the

* Corresponding author. Tel.: +44 7591848541.
E-mail address: psxjd3@nottingham.ac.uk (J. Duan).

http://dx.doi.org/10.1016/j.bspc.2015.09.012
1746-8094/

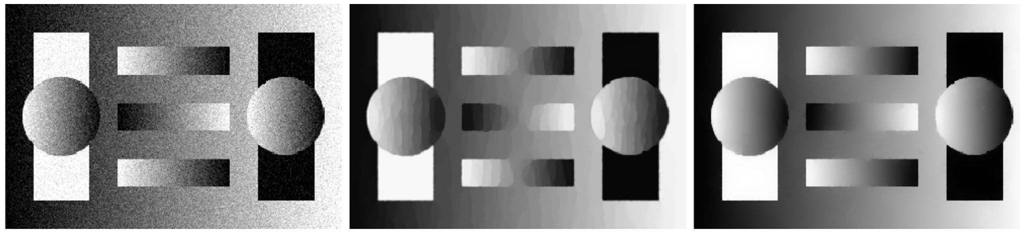

Fig. 1. Denoising a synthetic image with TV and TGV penalty. The noisy test image f (left), its TV regularisation (middle) and its TGV (right), which does not have the staircase effect.

Table 1
Methods and their abbreviations for comparison.

No.	Full name	Abbreviations
1	Hybrid median filter	HMF
2	Haar wavelet (hard thresholding)	HWT
3	Dual tree complex wavelet (soft thresholding)	DTCWT
4	Nonlinear complex diffusion filter	NCDF
5	Anisotropic coherent enhancing diffusion	ACED
6	Vese–Osher decomposition model	VO

OCT images which have produced better results than conventional wavelets.

Diffusion based approach can smooth images while preserving edges of objects and it often leads to partial differential equations (PDEs). Salinas et al. [16] compared the performance of Perona–Malik isotropic diffusion with a nonlinear complex diffusion filter for OCT denoising [17]. The nonlinear complex diffusion was combined with the anisotropic coherence enhancing diffusion [18] for noise reduction, segmentation and structure analysis in retinal OCT images. Bernardes et al. [19] proposed a new formulation of the nonlinear complex diffusion filter. One particular advantage of their method over the original nonlinear complex diffusion is that the conductance parameter k in their formulation can be adaptive to the OCT data automatically. Bernardes' method was then extended to 3D OCT image denoising with the GPU programming by Rodrigues et al. [20]. In addition, Puvanathasan et al. [21] presented the application of the interval type-II fuzzy anisotropic diffusion algorithm, where they considered the uncertainty in the calculated diffusion coefficient and appropriate adjustments to the coefficient were made. They also included edge information and a noise estimate in their formulation of the nonlinear isotropic diffusion for OCT speckle reduction.

Variational models offer powerful processing capabilities for imaging [22–27]. They have been widely used in the last two decades but have only been used recently for OCT image processing [23,28]. In this paper, based on the classical Vese–Osher (VO)

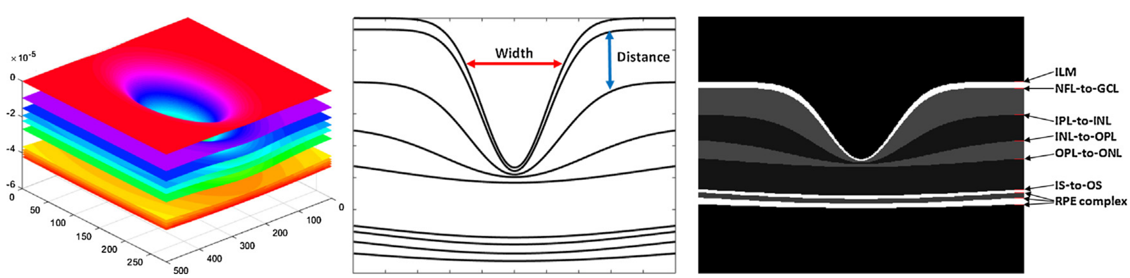

Fig. 2. Procedure of simulation for the synthetic OCT image. Left image: 3D sharp generated by Eq. (4.1); Middle image: The middle cross of the 3D sharp; Right image: Synthetic OCT image (B-scan) with 9 retinal layers. They are respectively ILM (internal limiting membrane), NFL (nerve fiber layer), GCL (ganglion cell layer), IPL (inner plexiform layer), INL (inner nuclear layer), OPL (outer plexiform layer), ONL (outer nuclear layer), IS (inner segment), OS (outer segment), and RPE (retinal pigment epithelium).

Table 2
Comparison of the PSNR, SNR, RMSE and SSIM using the different methods on the synthetic OCT image (i.e. Fig. 2 right) with 5 different noise variances.

	PSNR test					SNR test				
Noise variance	0.02	0.04	0.06	0.08	0.1	0.02	0.04	0.06	0.08	0.1
Noisy image	17.5325	14.9554	13.5430	12.5612	11.8256	8.4672	5.8901	4.7777	3.4959	2.7603
HMF	21.0741	20.2947	19.9165	19.4774	19.0066	12.0088	11.2294	10.8512	10.4121	9.9413
HWT	24.3981	22.1582	20.8430	19.3209	18.0995	15.3328	13.0929	11.7777	10.2556	9.0342
DTCWT	27.8702	24.7867	23.1115	21.9070	20.4468	18.8049	15.7214	14.0462	12.8417	11.3815
NCDF	20.9252	19.0848	18.4835	17.3998	16.8213	11.8599	10.0195	9.4182	8.3345	7.7560
ACED	28.1206	26.2074	24.6428	23.0592	21.4316	19.0553	17.1421	15.5775	13.9939	12.3664
VO	28.2919	26.4631	24.9032	23.5448	22.3510	19.2266	17.3978	15.8379	14.4795	13.2857
Ours	**32.0284**	**29.5787**	**27.4901**	**25.9198**	**24.4470**	**22.9631**	**20.5134**	**18.4248**	**16.8545**	**15.3817**

	RMSE test					SSIM test				
Noise variance	0.02	0.04	0.06	0.08	0.1	0.02	0.04	0.06	0.08	0.1
Noisy image	9.9006	10.3206	10.5214	10.6182	10.6609	0.1327	0.0978	0.0826	0.0730	0.0655
HMF	6.0263	6.5034	6.8127	7.0316	7.0406	0.6844	0.5745	0.4979	0.4496	0.4133
HWT	4.8105	4.9782	5.0147	5.0320	5.0487	0.9249	0.8923	0.8709	0.8369	0.8273
DTCWT	4.1782	4.4722	4.5374	4.5669	4.5834	0.9317	0.9094	0.8934	0.8730	0.8513
NCDF	4.7767	4.8449	4.8746	4.9408	5.0166	0.7998	0.7808	0.7781	0.7768	0.7722
ACED	5.0821	5.4730	5.4769	5.5201	5.5256	0.7679	0.6761	0.6016	0.5141	0.4654
VO	4.0315	4.0812	4.0943	4.0973	4.1099	0.9728	0.9624	0.9517	0.9394	0.9267
Ours	**3.7756**	**3.9375**	**3.9437**	**3.9456**	**3.9759**	**0.9871**	**0.9781**	**0.9684**	**0.9590**	**0.9481**